(Received 21 July 2025, Accepted 15 September 2025, Scheduled 25 September 2025)

A Monopole Antenna for 5G Sub-6 GHz and WLAN (Wi-Fi 5 and Wi-Fi 6) Band Applications

Zhengting Zhang[1], Han Lin[1,*], Chenlu Li[2], and Xiaoyan Wei[1]

[1] School of Electrical and Information Engineering, Anhui University of Science and Technology, Huainan 232001, China
[2] School of Electrical and Information Engineering, Hefei Normal University, Hefei 230061, China

ABSTRACT: In this paper, a novel monopole broadband dual-band antenna design for wireless communication systems is proposed, with its fabrication and experimental validation presented. To significantly enhance impedance matching performance, the antenna employs a T-shaped feed slot resonant structure integrated with symmetric L-shaped radiating patches. It covers critical Sub-6 GHz bands (N41/N77/N78/N79) along with Wi-Fi 5 and Wi-Fi 6 spectrums. Notably, the N41 band, as a core 5G frequency band, possesses advantages such as wide bandwidth, strong penetration capability, and flexible deployment, rendering it ideal for urban coverage and high-speed transmission. Experimental results demonstrate that the antenna achieves a −10 dB impedance bandwidth spanning 2.43–2.72 GHz and 3.31–7.32 GHz, with a peak gain of 5.48 dB under omnidirectional radiation characteristics. Its compact design is suitable for miniaturized terminal devices, exhibiting high practical value in 5G Sub-6 GHz and multi-band wireless communication applications.

1. INTRODUCTION

The advent of 5G technology has profoundly reshaped mobile user demands, ushering revolutionary changes through its provision of rapid data transfer, low latency, high capacity, and enhanced service capabilities. The evolution of 5G is driven by eight core factors: mobility, latency, spectrum efficiency, connection density, peak data rate, area traffic capacity, network energy efficiency, and user experienced data rate. These established standards aim to meet escalating communication requirements and the pervasive demands of internet of things (IoT) services [1, 2]. Within China, Sub-6 GHz frequency band encompassing N41, N77, N78, and N79 is widely adopted for its optimal balance of high speed and sufficient coverage, proving crucial for the nation's 5G development [3, 4].

Concurrently, rapid global population growth has precipitated a surge in mobile devices, each operating across distinct communication bands [5]. Consequently, designing single terminal devices capable of integrating multi-functional communication has become imperative [6]. In this context, monopole broadband antennas are increasingly recognized as an ideal solution [7], notably for their ability to cover the entire Sub-6 GHz spectrum. Furthermore, the integration of additional wireless communication bands, such as Wi-Fi 5 and Wi-Fi 6, is essential within these terminal devices. Research and development of monopole broadband antennas are therefore critical for building efficient modern communication networks.

Microstrip patch antennas are extensively utilized in diverse wireless systems owing to their low profile, compact size, and ease of design and fabrication [8–12]. Ref. [13] achieved coverage for 4G-LTE, WiMAX, WLAN, and S/C/X bands by etching rectangular slots on the ground plane and incorporating inverted T-shaped and E-shaped stubs, alongside slot etching on the feedline for improved impedance matching. Studies [9–12] developed microstrip multi-band antennas via slotting techniques on either radiating patch or ground plane. For instance, Reference [14] realized three-band coverage of GPS (1.575 GHz) and WLAN (2.4 GHz and 5.8 GHz) using an H-shaped slot antenna with microstrip coupled feeding, and achieved this by exciting monopole mode and slot mode, with a measured gain of 3.7 dB and being suitable for handheld devices. Ref. [15] proposed a dual-band reconfigurable antenna array, achieving the coverage of Sub-6 GHz (3.5 GHz) using radio frequency switches and phase shifters. In Sub-6 GHz band, an antenna selection architecture was adopted, with a 40% reduction in power consumption. Ref. [16] introduced a two-element ultra-wideband multiple-input multiple-output (UWB-MIMO) antenna with a rectangular stub achieving high isolation, extended UWB operation with a single wireless local area network (WLAN) band-notched function via open-loop slots in rectangular radiators. Ref. [17] introduced a novel common-ground stub structure achieving high isolation and gain, extended antenna operation from single to dual-band via etched L-shaped and inverted L-shaped slots, and enhanced bandwidth and gain using an etched annular ring with leaf-like structures. A dual-circularly polarized broadband U-slot antenna in [18] achieved a 1.8–6.61 GHz bandwidth and 3.8 dB peak gain. Refs. [19, 20] utilized ground plane slotting with L-shaped radiating patches for multi-band coverage, with [19] improving circular polarization performance via an added L-shaped branch within a square slot to cover GPS, 5G, and Wi-Fi 6E bands. Ref. [21] utilized a heterogeneous patch (circular + rectangular) structure to design a 16-element dual-band array antenna, covering 2.2–3.18 GHz and 4.81–7.21 GHz frequency bands, supporting multiple stan-

* Corresponding author: Han Lin (hanlin@aust.edu.cn).

dards including Bluetooth, Zigbee, WiMAX, and Wi-Fi-6, with a gain of 8.5 dB. Ref. [22] incorporated a J-shaped slot and parasitic elements into a planar inverted F-shape antenna (PIFA), achieving the dual-band coverage of 2.5 GHz (13% bandwidth) and 5.2 GHz (76% bandwidth), and supporting standards such as LTE, WLAN, and WiMAX. Ref. [23] presented a novel antenna combining Koch and Sierpinski fractal geometries, covering 5G/WLAN and navigation bands through multiple etched triangular slots on the radiator, albeit with complex fabrication challenges.

Despite these advancements, existing multi-band antennas still have limitations: for example, those in [19, 21] either fail to cover the critical N41 band or lack sufficient gain for high-speed transmission, while [29] (focusing on MIMO diversity) exhibits lower gain (< 5 dB) in key frequency segments. Meanwhile, although the fractal-based design in [23] achieves wide coverage, its complex geometric structure increases manufacturing difficulty and cost, hindering its application in low-cost, miniaturized terminals.

To address these gaps, this paper proposes a structurally simple, dual-band, high-gain monopole broadband antenna design based on an FR-4 substrate. Its innovations lie in three aspects. Firstly, a modified circular radiating patch with an etched horseshoe-shaped slot enables effective bandwidth extension without relying on complex fractal structures, simplifying fabrication while ensuring dual-band operation. Secondly, symmetric L-shaped metallic patches integrated alongside the T-shaped feedline optimize impedance matching across both Sub-6 GHz (N41/N77/N78/N79) and Wi-Fi 5/6 bands, enhancing performance stability across multi-standards. Thirdly, with compact dimensions of 38 mm $\times$ 26 mm $\times$ 0.8 mm, it is well suited for miniaturized terminal devices, bridging the gap between multi-standard compatibility and structural miniaturization. Simulation results obtained using High Frequency Structure Simulator (HFSS) software indicate that this symmetrical antenna structure effectively covers the target bands while demonstrating favorable gain characteristics.

2. ANTENNA DESIGN

2.1. Antenna Geometry

The antenna structure design is depicted in Figure 1. The antenna is fed by a 50 Ω microstrip line, with tinned radiating patches printed on an FR-4 substrate (relative permittivity $= 4.4$, loss tangent $= 0.02$). The overall dimensions measure 38 mm $\times$ 26 mm $\times$ 0.8 mm. The top layer comprises a T-shaped microstrip feedline and a modified circular radiator. The circular radiating patch is primarily selected for its inherent omnidirectional radiation characteristic in the azimuthal plane, which meets the requirement for uniform coverage in IoT and urban 5G scenarios. Additionally, its continuous perimeter facilitates flexible slotting (such as the horseshoe-shaped slot adopted in this design) to adjust the current path, enabling dual-band operation without compromising structural compactness. Compared with rectangular patches, the circular structure exhibits a smoother current distribution, which reduces edge diffraction and improves impedance stability across all

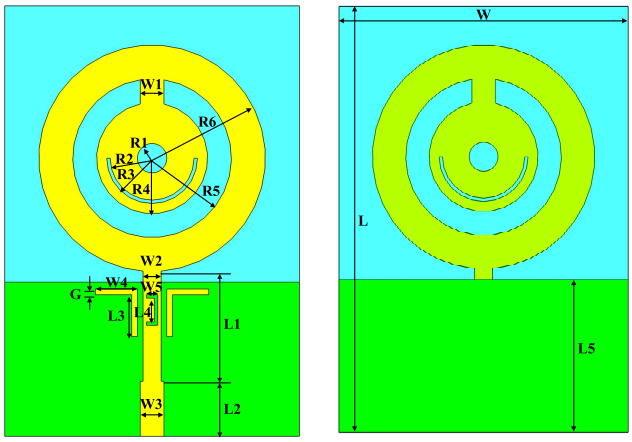

FIGURE 1. Geometry and parameters of the proposed antenna.

operating frequency bands, a design choice that lays the foundation for subsequent structural optimizations. The bottom layer features a rectangular metallic ground plane. To further enhance bandwidth, the circular patch geometry is modified: by etching a horseshoe-shaped slot into the radiator (consistent with the slotting advantage of the circular structure mentioned above), the antenna bandwidth is effectively increased while simultaneously achieving dual-band operation. Furthermore, a quarter-wavelength impedance transformer section is employed to improve impedance matching, and two symmetrical L-shaped metallic patches are integrated alongside the T-shaped microstrip feedline to augment this matching effect. The feasibility of this design approach from the selection of the circular radiating patch to the implementation of slotting and impedance optimization is validated through both simulation and measurement results. All design parameters are detailed in Table 1.

TABLE 1. Recommended design dimensions for antenna.

Parameter	Value/mm	Parameter	Value/mm
W	26.0	$W3$	2.1
L	38.0	$W4$	3.5
$R1$	1.3	$W5$	1.0
$R2$	3.7	$L1$	9.7
$R3$	4.0	$L2$	4.9
$R4$	4.9	$L3$	3.9
$R5$	7.0	$L4$	2.1
$R6$	10.0	$L5$	13.6
$W1$	2.1	G	0.5
$W2$	1.6	H	0.8

2.2. Evolution of Multi-Frequency Antennas

The design evolution of the antenna, as illustrated in Figures 2 and 3, demonstrates the S-parameter performance of Ant 1–Ant 4. The initial structure, depicted in Figure 2(a), consists of a rectangular ground plane, a microstrip feed line, and a key-shaped radiating element, denoted as Ant 1. As shown in Figure 3, the simulation results of this configuration achieve dual-band operation covering the frequency ranges of 2.43–2.72 GHz and 3.31–7.32 GHz. To broaden the bandwidth, a

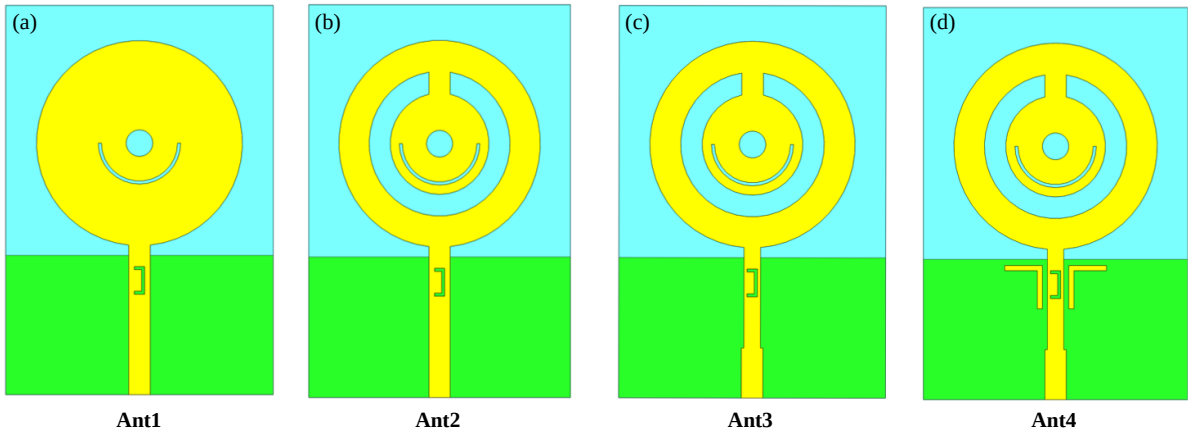

FIGURE 2. The design development of the antenna structure (a) Ant 1, (b) Ant 2, (c) Ant 3 and (d) Ant 4.

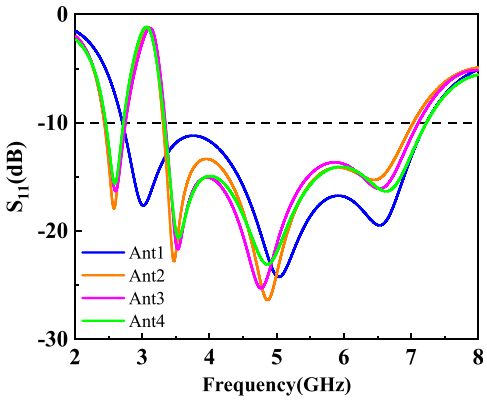

FIGURE 3. Simulated results for Ant 1–Ant 4.

horseshoe-shaped slot is etched on the upper portion of the key-shaped patch in the initial design to modify the current path or extend the current flow, thereby generating resonance at approximately 2.6 GHz. The introduced horseshoe structure alters the strong current distribution in that region, facilitating better excitation of the desired modes and contributing to bandwidth expansion, as illustrated in Figure 2(b). From the corresponding S-parameter results, it is evident that this modification significantly enhances the bandwidth in the Sub-6 GHz band compared to Ant 1, particularly covering the N41 band. Furthermore, by incorporating a 1/4-wavelength impedance matching section, the matching bandwidth is further widened, resulting in an additional resonant frequency around 4.9 GHz. As inferred from S-parameters of Ant 3 and Ant 4, implementing symmetric L-shaped patches on both sides of the feedline improves the impedance matching performance. Ultimately, the final optimized antenna structure achieves dual-wideband coverage with operational bandwidths of 2.43–2.72 GHz and 3.31–7.32 GHz, meeting the requirements for modern multi-band wireless communication systems.

3. PARAMETRIC ANALYSES

To investigate the impact of different antenna parameters on its performance, a systematic study was conducted to clarify manufacturing tolerances and, more importantly, to identify how parameters influence bandwidth. Based on the antenna's structural features and design goals, four key parameters were analyzed: the length of $L2$ in the T-shaped microstrip, the opening size $W1$ of the horseshoe-shaped slot, the ground plane height $L5$, and the thickness H of the FR-4 substrate. Among them, $L2$ and $W1$ form the basic structure of the antenna and are directly related to the design evolution process, while $L5$ and H are critical for impedance matching optimization, particularly in high-frequency bands.

Figure 4(a) illustrates the effect of $L2$ on resonance points: when $L2 = 1.9$ mm, only two resonance points are generated, failing to meet the requirement for resonance at 4.9 GHz; as $L2$ increases, resonance emerges around 4.9 GHz, and $L2 = 4.9$ mm was finally selected for better matching performance. Figure 4(b) shows the significant impact of $W1$ (opening size of the horseshoe-shaped slot) on the overall frequency range and high frequencies: when $W1 = 1.1$ mm or 5.1 mm, the bandwidth below -10 dB fails to cover the designed frequency band, resulting in poor performance; $W1 = 2.1$ mm, however, provides better matching and thus was chosen as the optimal parameter.

The influence of $L5$ on S_{11} parameter is presented in Figure 4(c), with notable effects on high-frequency bands (especially around 6.7 GHz): when $L5 = 13.6$ mm, the antenna achieves optimal impedance matching at 6.7 GHz (S_{11} well below -10 dB); a shorter $L5$ (12.6 mm) shifts the resonance to higher frequencies, while a longer $L5$ (14.6 mm) shifts it to lower frequencies, both degrading matching at 6.7 GHz. It indicates that $L5$ is critical for ensuring good matching in high-frequency bands.

Figure 4(d) shows the effect of H on S_{11} parameter. The thickness of the FR-4 substrate alters the coupling strength between the radiating patch and ground plane: when $H = 0.8$ mm, the antenna exhibits excellent matching across the entire operating bandwidth (including 6.7 GHz); a thinner substrate ($H = 0.6$ mm) enhances coupling, narrowing the high-frequency bandwidth and degrading matching at 6.7 GHz; a thicker substrate ($H = 1.0$ mm) weakens coupling, causing res-

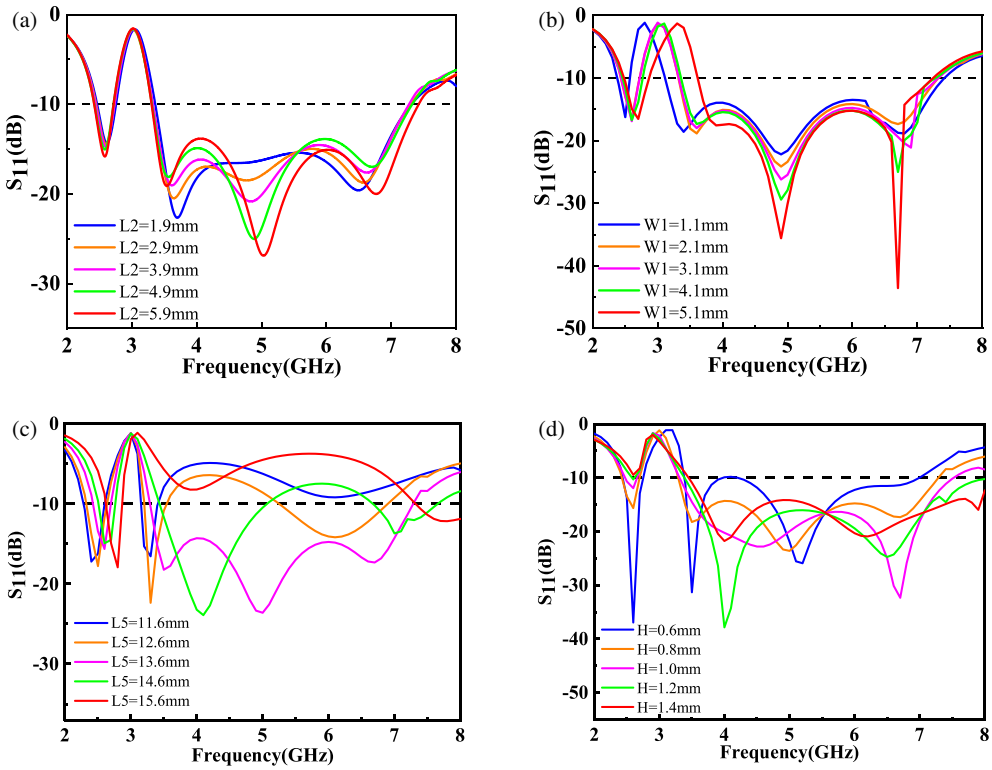

FIGURE 4. The effect of adjusted parameters on S_{11} parameters (a) $L2$, (b) $W1$, (c) $L5$, (d) H.

onance shift and poor matching at 6.7 GHz. Thus, $H = 0.8$ mm is optimal for maintaining good impedance performance.

In summary, parametric optimization confirms that $L2 = 4.9$ mm, $W1 = 2.1$ mm, $L5 = 13.6$ mm, and $H = 0.8$ mm form the optimal combination, ensuring good impedance matching across the target bands, especially stable performance in the high-frequency region around 6.7 GHz. These parameters were adopted in the final design.

4. SURFACE CURRENT DISTRIBUTIONS

Figure 5 illustrates the surface current distribution of the antenna under resonant modes, offering insights into how structural modifications influence radiation behavior. As observed in Figure 5(a), the surface current is uniformly distributed at 2.6 GHz, indicating excellent radiation performance at this frequency. From Figure 5(b), the etched horseshoe-shaped slot resonates at 3.5 GHz, a key feature enabling dual-band operation. Among the design evolutions, the role of the L-shaped stubs in Ant 4 is particularly noteworthy: while their impact on S-parameter curves (as shown in Figure 3) appears subtle, their regulation of current distribution is pivotal for optimizing antenna performance.

As depicted in Figure 5(c), at 4.9 GHz, currents are significantly concentrated near the L-shaped patches, a distribution that enhances capacitive coupling with the feedline. This concentrated current effect directly improves impedance matching, as confirmed by the optimized performance in the 4.5–5.5 GHz band. Compared to Ant 3, this improvement extends the upper bandwidth by 0.8 GHz, expanding the antenna's coverage of high-frequency spectra.

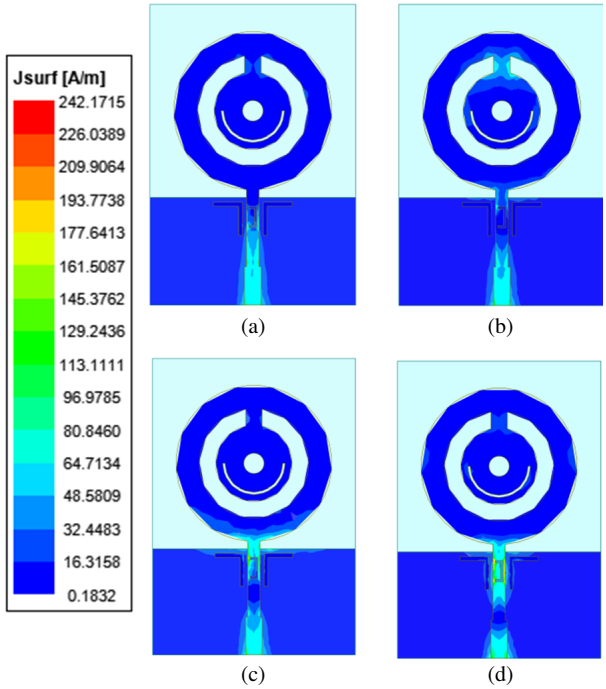

FIGURE 5. Current distribution at resonance point: (a) 2.6 GHz, (b) 3.5 GHz, (c) 4.9 GHz, (d) 6.7 GHz.

Furthermore, the L-shaped stubs introduce a secondary resonance at 6.7 GHz, as evidenced by the current distribution in Figure 5(d). This additional resonance is critical for covering

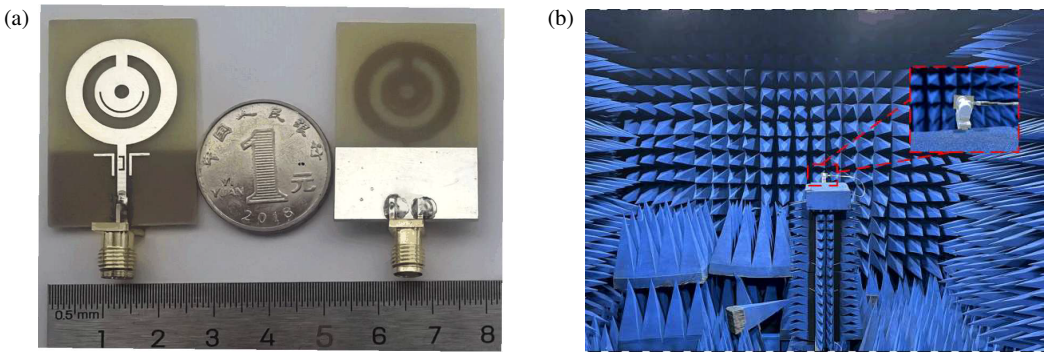

FIGURE 6. Fabrication and measurement: (a) front and back view of the proposed antenna; (b) far-field measurement in an anechoic chamber.

the Wi-Fi 6E high-frequency band, thereby enhancing the antenna's multi-band adaptability. Together, these observations highlight that even subtle structural adjustments, such as the integration of L-shaped stubs, can profoundly influence current paths, ultimately boosting the antenna's functionality in diverse wireless communication scenarios.

5. MEASUREMENT AND DISCUSSION

5.1. S-Parameter Results

The fabricated prototype is shown in Figure 6(a), while the test environment of the antenna is illustrated in Figure 6(b). The S-parameters were measured using an AV3629D vector network analyzer. We note the slight misalignment of the SMA connector in Figure 6(a), which introduced an unexpected impedance discontinuity at the feed interface. Post-measurement analysis confirmed that this misalignment directly caused resonant frequency shifts: specifically, compared to simulation results, the resonant points at 3.5 GHz and 4.9 GHz critical frequencies within the Sub-6 GHz band shifted rightward by approximately 0.5 GHz.

To address this issue, we implemented targeted calibration using AV3629D's impedance compensation algorithm, which adjusted for the discontinuity induced by mechanical offset by extending the reference plane. After calibration, the shifted resonant points were corrected to within 0.08 GHz of the simulated values, and the overall S_{11} curves showed good agreement with simulations across the operating bands (2.43–2.72 GHz and 3.31–7.32 GHz), with a maximum deviation of ± 0.6 dB consistent with typical fabrication tolerances for microstrip antennas.

The measured data in Figure 7 clearly indicate that the developed antenna has successfully achieved dual-band coverage, with specific frequency ranges of 2.43–2.72 GHz and 3.31–7.32 GHz. The coverage characteristics of these two frequency bands provide fundamental support for the multi-scenario applications of the antenna.

It should be noted that, in addition to the SMA misalignment addressed above, slight discrepancies between simulated results and measured data also stem from other process errors in manufacturing (e.g., deviations in dielectric substrate size, insufficient etching precision of conductor patterns) and potential

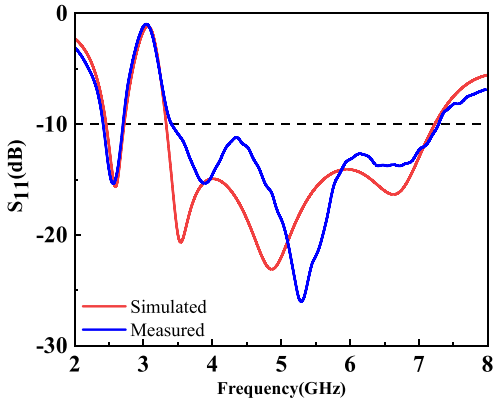

FIGURE 7. Simulated and measured S-parameters.

welding issues (e.g., irregular solder joints, fluctuations in contact impedance at feeding points). However, after calibration for the SMA misalignment, repeated measurements ($n = 5$) showed high consistency with a standard deviation of < 0.3 dB, confirming that the corrected data reliably reflects the antenna's inherent performance. Overall, the frequency bands covered by the antenna maintain strong consistency between simulation predictions and actual tests, fully verifying the rationality of the antenna design scheme and its engineering feasibility.

5.2. Far-Field Characteristics

The radiation patterns of the antenna were measured in an anechoic chamber. The measurement results and simulation data are summarized in Figures 8(a)–(d), which clearly present a comparison of the antenna's radiation characteristics in the XOZ and YOZ planes at four key frequency points (2.6 GHz, 3.5 GHz, 4.9 GHz, and 6.7 GHz).

In the XOZ plane, the radiation pattern is predominantly bidirectional, with two main radiation directions symmetrically distributed and relatively concentrated gain. This directivity enables the electromagnetic energy to be radiated intensively toward specific directions, which not only enhances signal strength in target directions (suitable for point-to-point directional communication) but also reduces energy waste in non-target directions, helping to suppress interference. In the YOZ plane, the antenna exhibits overall omnidirectional radiation characteristics, with approximately uniform radiation intensity

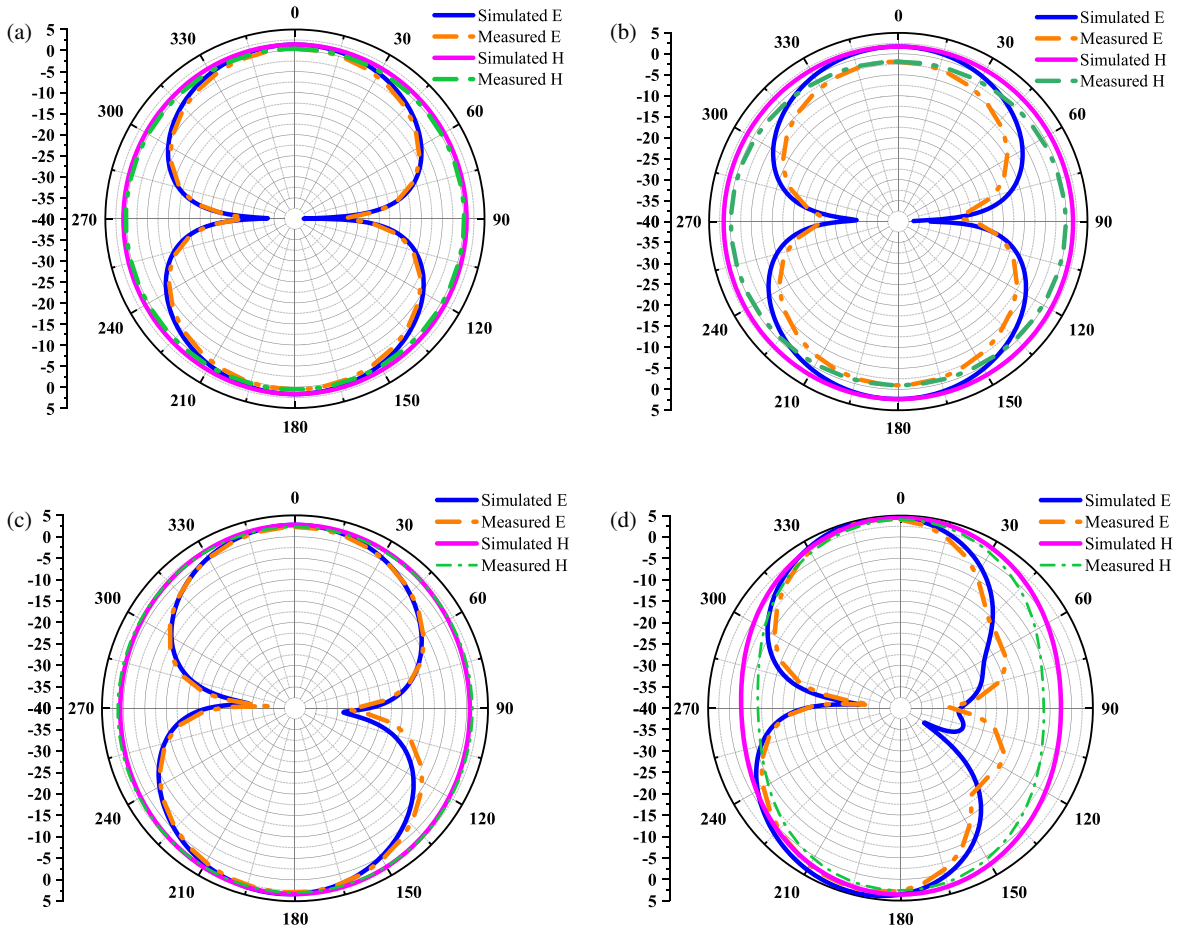

FIGURE 8. Simulated and measured far-field patterns on E and H planes at: (a) 2.6 GHz, (b) 3.5 GHz, (c) 4.9 GHz, (d) 6.7 GHz.

within the 360° azimuth range. This facilitates full-range signal coverage, making it suitable for scenarios requiring comprehensive coverage such as indoor distributed communication systems or IoT nodes.

However, as shown in Figure 8(d), the far-field radiation performance at 6.7 GHz is relatively poor. Analysis indicates that this is directly related to the backplane design and substrate thickness. The backplane width of this monopole antenna is $L5 = 13.6$ mm, which corresponds to approximately 0.3λ at the 6.7 GHz high frequency. This width causes current to concentrate at the edges, easily inducing significant parasitic radiation, thereby reducing the main lobe gain by approximately 1.0 dB and increasing the sidelobe level by 1.4 dB. This is consistent with the previously discussed influence of $L5$ on the S_{11} parameter, while $L5 = 13.6$ mm ensures good impedance matching at 6.7 GHz. The narrow width exacerbates current reflection and scattering at high frequencies, thus affecting far-field performance. Additionally, the substrate thickness $H = 0.8$ mm limits high-frequency radiation efficiency, and this thickness is only about 1/70 of the wavelength corresponding to 6.7 GHz. The excessively short spacing enhances electromagnetic coupling between the radiator and backplane, leading to partial energy absorption by the backplane instead of outward radiation, which further impairs far-field performance.

Furthermore, there are differences in the far-field patterns between horizontal polarization (XOZ plane) and vertical polarization (YOZ plane) at 6.7 GHz: the gain deviation in the main lobe direction ($\theta = 0°$) is less than 0.4 dB, but the difference reaches 1.7 dB in the sidelobe regions ($\theta = \pm 60°$). This is mainly because the narrow backplane ($L5 = 13.6$ mm) imposes stronger constraints on horizontal polarization currents, and the asymmetric coupling between the L-shaped stub and backplane at $H = 0.8$ mm causes horizontal polarization to be susceptible to interference from parasitic modes. These phenomena are all results of sacrificing high-frequency radiation performance to achieve excellent impedance matching.

Within the effective operating frequency band, the antenna gain varies dynamically between 1 and 6 dB, reaching a peak of 5.48 dB at 7.2 GHz (as shown in Figure 9). Despite certain fluctuations, the overall performance remains stable without abrupt changes or abnormal attenuation. In addition, the voltage standing wave ratio (VSWR) within the operating band is less than 2 (as shown in Figure 11), indicating good impedance matching. The radiation efficiency is also excellent: in the 2.43–2.72 GHz band, the efficiency decreases slightly with increasing frequency but remains around 95%; in the 3.31–7.32 GHz band, it avoids the detuning valley near 3 GHz and stabilizes at approximately 95% (as shown in Figure 10). The overall per-

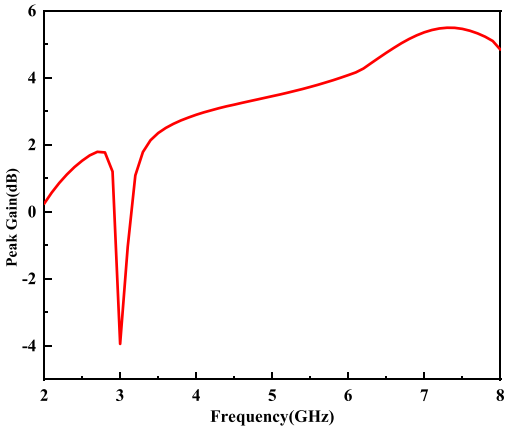

FIGURE 9. Peak gain of the proposed antenna.

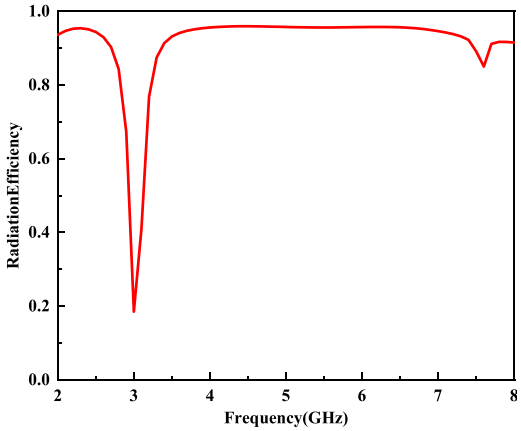

FIGURE 10. Radiation efficiency of the proposed antenna.

TABLE 2. Antenna parameter comparison.

Ref.	Size (mm^2)	Peak Gain (dB)	Bandwidth (GHz)	Applications
[8]	20 × 35	3.52	5.5356–7.0449	WLAN
[6]	25 × 15	4.1	4–7.8, 3.3–4.2, 5.8–7.2, 3.3–4.2	WiMAX, WAVE
[10]	6.5 × 12.9	3.2	2.3–4.0, 5–6.6	WLAN, WiMAX
[9]	32 × 18	4.5	1.7–2.1, 2.4–2.7, 3.3–3.6, 5.0–5.7	GSM, Bluetooth, WLAN, WiMAX
[24]	46 × 30	1.36	1.85–3.63, 5.07–7.96	LTE, Bluetooth, WAP, ISM, WLAN
[11]	46 × 44	1.76	5.8–7.2	WLAN, Sub-6 GHz 5G
[25]	20 × 14.75	7.93, 4.23, 7.57	2.38–3.0, 3.21–3.61, 5.02–6.18	WLAN, WiMAX
[28]	75 × 150	5.4	3.0–6.37	Sub-6 GHz 5G(N77/N78/N79)
[29]	25 × 30	4.2	3.12–7.12	Sub-6 GHz 5G(N77/N78/N79), Wi-Fi 5, Wi-Fi 6
[30]	72 × 72	2.5	3.30–6.0	Sub-6 GHz 5G(N77/N78/N79), WLAN
[27]	55 × 55	4	3.34–5.01, 8.9–9.2	Sub-6 GHz 5G, X
[26]	80 × 150	2,2.5	3.6–3.8, 5.15–5.92	LTE 42/43/46
[23]	80 × 54	4.64	0.85–0.96, 1.22–1.54, 1.86–2.12, 2.4–3.22, 3.69–3.97, 4.84–5.98	2G/3G/4G/5G, WLAN, navigation
This work	38 × 26	5.48	2.43–2.72, 3.31–7.32	Sub-6 GHz 5G(N41/N77/N78/N79), Wi-Fi 5, Wi-Fi 6

formance meets the requirements of wireless communication applications.

5.3. Comparative Study

Table 2 details a comparison of the proposed antenna with previously published works in terms of size, peak gain, bandwidth, and applications. To highlight its innovation, references are ordered by "technology evolution": progressing from single-application or single-band, to partially multi-standard with limitations, then to 5G-oriented but incompletely covered, culminating in the proposed work.

Early single-application or single-band antennas [6, 8, 10] support only limited standards (e.g., WLAN, WiMAX) with narrow applicability. Transitional multi-standard antennas [9, 11, 24, 25] attempt multi-standard support but suffer from deficiencies: fragmented bandwidth, low gain (1.36–4.5 dB), or incomplete size-performance balance. Advanced 5G-oriented antennas [23, 26–30] focus on 5G but lack full compatibility — some are oversized (e.g., [23] at $80 \times 54\ mm^2$), and others have limited band coverage.

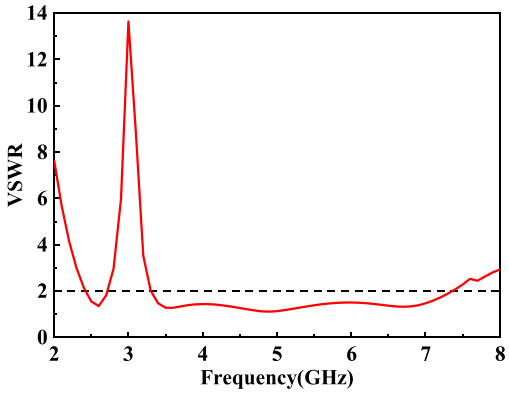

FIGURE 11. VSWR of the proposed antenna.

In contrast, the proposed antenna achieves breakthroughs: it covers Sub-6 GHz 5G (N41/N77/N78/N79), Wi-Fi 5, and Wi-Fi 6 for full compatibility, offers a peak gain of 5.48 dB (superior to most compared works), features comprehensive bandwidth (2.43–2.72, 3.31–7.32 GHz), and has a compact size ($38 \times 26\,\text{mm}^2$, smaller than [11, 23, 24, 26–28]). It thus balances full-scenario compatibility, high performance, and compactness, making it ideal for miniaturized terminals.

6. CONCLUSIONS

This paper presents a compact dual-band monopole antenna with omnidirectional radiation characteristics, covering Sub-6 GHz 5G bands (N41/N77/N78/N79) and Wi-Fi 5/6 bands. Key achievements include a circular patch with a horseshoe-shaped slot enabling bandwidth extension, L-shaped stubs optimizing impedance matching, and a peak gain of 5.48 dB achieved on an FR-4 substrate. Limitations involve slightly reduced efficiency at 6.7 GHz and fixed polarization, while future work will focus on research into reconfigurable slots to achieve polarization adaptivity and extend coverage to the mmWave band.

ACKNOWLEDGEMENT

This work was supported by the Fund of Anhui Mining Machinery and Electrical Equipment Coordination Innovation Center (Anhui University of Science and Technology) under grant No. KSJD202406.

REFERENCES

[1] Lee, J., E. Tejedor, K. Ranta-Aho, H. Wang, K.-T. Lee, E. Semaan, E. Mohyeldin, J. Song, C. Bergljung, and S. Jung, "Spectrum for 5G: Global status, challenges, and enabling technologies," *IEEE Communications Magazine*, Vol. 56, No. 3, 12–18, Mar. 2018.

[2] Deng, D.-J., S.-Y. Lien, C.-C. Lin, M. Gan, and H.-C. Chen, "IEEE 802.11ba wake-up radio: Performance evaluation and practical designs," *IEEE Access*, Vol. 8, 141 547–141 557, Jul. 2020.

[3] Liu, G., X. Hou, Y. Huang, H. Shao, Y. Zheng, F. Wang, and Q. Wang, "Coverage enhancement and fundamental performance of 5G: Analysis and field trial," *IEEE Communications Magazine*, Vol. 57, No. 6, 126–131, Jun. 2019.

[4] Miao, H., J. Zhang, P. Tang, L. Tian, X. Zhao, B. Guo, and G. Liu, "Sub-6 GHz to mmWave for 5G-advanced and beyond: Channel measurements, characteristics and impact on system performance," *IEEE Journal on Selected Areas in Communications*, Vol. 41, No. 6, 1945–1960, Jun. 2023.

[5] Faouri, Y. S., S. Ahmad, N. O. Parchin, C. H. See, and R. Abd-Alhameed, "A novel meander bowtie-shaped antenna with multi-resonant and rejection bands for modern 5G communications," *Electronics*, Vol. 11, No. 5, 821, 2022.

[6] Awan, W. A., S. I. Naqvi, W. A. E. Ali, N. Hussain, A. Iqbal, H. H. Tran, M. Alibakhshikenari, and E. Limiti, "Design and realization of a frequency reconfigurable antenna with wide, dual, and single-band operations for compact sized wireless applications," *Electronics*, Vol. 10, No. 11, 1321, 2021.

[7] Zebiri, C., D. Sayad, I. Elfergani, A. Iqbal, W. F. A. Mshwat, J. Kosha, J. Rodriguez, and R. Abd-Alhameed, "A compact semi-circular and arc-shaped slot antenna for heterogeneous RF front-ends," *Electronics*, Vol. 8, No. 10, 1123, 2019.

[8] Paul, L. C., S. S. A. Ankan, T. Rani, M. T. R. Jim, M. Karaaslan, S. A. Shezan, and L. Wang, "Design and characterization of a compact four-element microstrip array antenna for WiFi-5/6 routers," *International Journal of RF and Microwave Computer-aided Engineering*, Vol. 2023, No. 1, 6640730, 2023.

[9] Zehforoosh, A. and Y. Zehforoosh, "Evaluation of a novel hook-shaped multiband monopole antenna based on the AHP method," *IET Communications*, Vol. 16, No. 3, 266–273, 2022.

[10] Huang, H., Y. Liu, S. Zhang, and S. Gong, "Multiband metamaterial-loaded monopole antenna for WLAN/WiMAX applications," *IEEE Antennas and Wireless Propagation Letters*, Vol. 14, 662–665, 2015.

[11] Gao, F. and H. Sun, "A radiation-pattern reconfigurable antenna array for vehicular communications," *Sensors*, Vol. 24, No. 13, 4136, 2024.

[12] Qing, X. and Z. N. Chen, "Compact asymmetric-slit microstrip antennas for circular polarization," *IEEE Transactions on Antennas and Propagation*, Vol. 59, No. 1, 285–288, 2011.

[13] Sah, B. K., G. Singla, and S. Sharma, "Design and development of enhanced bandwidth multi-frequency slotted antenna for 4G-LTE/WiMAX/WLAN and S/C/X-band applications," *International Journal of RF and Microwave Computer-Aided Engineering*, Vol. 30, No. 7, e22214, 2020.

[14] Chang, T.-H. and J.-F. Kiang, "Compact multi-band H-shaped slot antenna," *IEEE Transactions on Antennas and Propagation*, Vol. 61, No. 8, 4345–4349, 2013.

[15] Chen, K., C. Qi, and O. A. Dobre, "DBRAA: Sub-6 GHz and millimeter wave dual-band reconfigurable antenna array for ISAC," *IEEE Transactions on Communications*, Vol. 73, No. 5, 3215–3228, 2025.

[16] Haripriya, D., S. Venkatakiran, and A. Gokulachandar, "UWB-MIMO antenna of high isolation two elements with WLAN single band-notched behavior using roger material," *Materials Today: Proceedings*, Vol. 62, 1717–1721, 2022.

[17] Kumar, A., N. K. Narayaswamy, H. V. Kumar, B. Mishra, S. A. Siddique, and A. K. Dwivedi, "High-isolated WiFi-2.4 GHz/LTE MIMO antenna for RF-energy harvesting applications," *AEU — International Journal of Electronics and Communications*, Vol. 141, 153964, 2021.

[18] Xu, R., J.-Y. Li, J.-J. Yang, K. Wei, and Y.-X. Qi, "A design of U-shaped slot antenna with broadband dual circularly polarized radiation," *IEEE Transactions on Antennas and Propagation*, Vol. 65, No. 6, 3217–3220, 2017.

[19] Liu, X., H. Wang, X. Yang, and J. Wang, "Quad-band circular polarized antenna for GNSS, 5G and WIFI-6E applications," *Elec-*

tronics, Vol. 11, No. 7, 1133, 2022.

[20] Xu, R., J. Li, Y.-X. Qi, Y. Guangwei, and J.-J. Yang, "A design of triple-wideband triple-sense circularly polarized square slot antenna," *IEEE Antennas and Wireless Propagation Letters*, Vol. 16, 1763–1766, 2017.

[21] Paul, L. C., M. H. Ali, T. Rani, H. K. Saha, and M. T. R. Jim, "A sixteen-element dual band compact array antenna for ISM/Bluetooth/Zigbee/WiMAX/WiFi-2.4/5/6 GHz applications," *Heliyon*, Vol. 8, No. 11, e11675, 2022.

[22] El Halaoui, M., A. Kaabal, H. Asselman, S. Ahyoud, and A. Asselman, "Dual-band planar inverted-F antenna with enhanced bandwidth by adding a T-shaped slot and a two elements for mobile phone applications," *Progress In Electromagnetics Research C*, Vol. 59, 149–158, 2015.

[23] Yu, Z., J. Yu, X. Ran, and C. Zhu, "A novel Koch and Sierpinski combined fractal antenna for 2G/3G/4G/5G/WLAN/navigation applications," *Microwave and Optical Technology Letters*, Vol. 59, No. 9, 2147–2155, 2017.

[24] Tiwari, R. N., P. Singh, S. Pandey, R. Anand, D. K. Singh, and B. K. Kanaujia, "Swastika shaped slot embedded two port dual frequency band MIMO antenna for wireless applications," *Analog Integrated Circuits and Signal Processing*, Vol. 109, No. 1, 103–113, 2021.

[25] Kumar, M. and V. Nath, "Design and development of triple-band compact ACS-fed MIMO antenna for 2.4/3.5/5 GHz WLAN/WiMAX applications," *Analog Integrated Circuits and Signal Processing*, Vol. 103, No. 3, 461–470, 2020.

[26] Aziz, H. S. and D. K. Naji, "Compact dual-band MIMO antenna system for LTE smartphone applications," *Progress In Electromagnetics Research C*, Vol. 102, 13–30, 2020.

[27] Kulkarni, N. P., N. B. Bahadure, P. D. Patil, and J. S. Kulkarni, "Flexible interconnected 4-port MIMO antenna for Sub-6 GHz 5G and X band applications," *AEU — International Journal of Electronics and Communications*, Vol. 152, 154243, 2022.

[28] Joseph, J. and G. S. Let, "A wideband uniplanar ground-centered dual-polarized quad MIMO for Sub-6 GHz 5G bands," *Arabian Journal for Science and Engineering*, Vol. 48, No. 11, 15 139–15 152, 2023.

[29] Addepalli, T., "Compact MIMO diversity antenna for 5G Sub: 6 GHz (N77/N78 and N79) and WLAN (Wi-Fi 5 and Wi-Fi 6) band applications," *Wireless Personal Communications*, Vol. 132, No. 3, 2203–2223, 2023.

[30] Addepalli, T., M. S. Kumar, C. R. Jetti, N. K. Gollamudi, B. K. Kumar, and J. Kulkarni, "Fractal loaded, novel, and compact two- and eight-element high diversity MIMO antenna for 5G Sub-6 GHz (N77/N78 and N79) and WLAN applications, verified with TCM analysis," *Electronics*, Vol. 12, No. 4, 952, 2023.